Hindawi
Geofluids
Volume 2020, Article ID 8880091, 12 pages
https://doi.org/10.1155/2020/8880091

Research Article

Coal and Gas Outburst Affected by Law of Small Fault Instability during Working Face Advance

Jianyun Lin,[1,2] **Yujun Zuo**,[1,2] **Kai Zhang**,[1] **Wenjibin Sun**,[1,2] **Biao Jin**,[1] **Taotao Li**,[1] **and Qing-gang Chen**[1]

[1]*Mining College, Guizhou University, Guiyang 550025, China*
[2]*School of Resource and Environmental Engineering, Guizhou University, Guiyang 550025, China*

Correspondence should be addressed to Yujun Zuo; zuo_yujun@163.com

Received 4 August 2020; Accepted 30 September 2020; Published 28 October 2020

Academic Editor: Zhijie Wen

To analyze the effect of small faults in the working face on coal and gas outbursts, the coal and gas outburst accident in the 2143_1 working face was studied with the 3DEC numerical simulation method, and the main research contents were the change laws of both stresses at the small fault and the overburden strata movement rate in the small fault zone of which the drop height and the strike were designed into different groups. The results show that the risk of small fault slip increases with the advancing working face. In addition, there is a positive correlation between the risk and the small fault throw. The movement rate of overburden strata in the small fault zone increases along with the rising of the small fault throw, which increases the energy transferred to the coal seam from the surrounding rock under the effect of the small fault. Hence, the effect of small faults on the working face on coal and gas outbursts was positively correlated with the small fault throw. Under the influence of a small fault strike, the closer it is to the small fault along the dip distance at the same working face, the greater the risk will be of a coal and gas outburst. And the bigger the small fault strike is, the greater is the stress concentration degree in front of the working face and the more the elastic energy is stored and the greater is the possibility of an outburst. The paper analyzes the influence of small faults on coal and gas outbursts in the working face, which has reference significance for the prediction and prevention of coal and gas outburst disaster in the working face.

1. Introduction

In the production process of coal mines, the small fault is one of the major geological problems that have troubled mine production for a very long time. Due to the small fault structure of the mining face, even under low gas condition, coal and gas outbursts in the mining face are still frequent. By a statistic of the distribution rule of gas disasters in mining areas, it is found that the fault structure is closely related to the occurrence of the outburst [1–4]. According to relevant statistics, nearly 80% of coal and gas outburst accidents are caused by small faults [5, 6], and these outburst accidents mostly occurred at coal roadway heading faces, followed by open-off cut, raise and dip, uncovering coal seam in the crosscut, mining face, and rock roadway heading face [7, 8].

Coal and gas outbursts have been a major geological hazard to underground coal mining for over 150 years and continue to cause serious problems all over the world [9–12]. Coal and gas outbursts are extremely violent dynamic disasters [13]. The research from Guo et al. [14] believed that the prominent influencing factors changed from three to four, that is, the tectonic stress field, the physical and mechanical properties of tectonic coal, coal seam gas, and structural combination characteristics. The influence of tectonic, geostatic, and mining stresses on coal and gas outbursts (CGO) becomes more obvious with increasing mining depth [15–18]. Liu et al. [19] established a mechanical analysis model of the expansion and evolution of the plastic zone in front of the driving face by numerical simulation method, analyzed the characteristics of the expansion and evolution of the plastic zone in front of the driving face, and discussed the physical and mechanical process and basic conditions of the development of coal and gas explosion caused by the evolution of the plastic zone. Zhang and Lowndes [20] used fault

tree coupling analysis (FTA) and an artificial neural network (ANN) model to predict the potential risk of a coal and gas outburst during underground mining of thick and deep coal seams in China. Zhai et al. [21] and Gong and Guo [22] statistically analyzed the 153 outburst accidents in the Pingdingshan mining region. The results indicate that the outburst accidents in this mining region were primarily influenced by the following factors: geological structure, mining depth, and the lithology of the roof and floor. In particular, gas outburst accidents of the highest frequency and intensity were reported in regions where geological structures were developed. Through the analysis of gas occurrence in the Pingdingshan mining area, Wang et al. [23] found that the in situ stress plays a leading role in the no. 8, 10, and 12 coal and gas outbursts and the outburst risk is the greatest. Chen et al. [24] took the Zhaozhuang coal mine as the research object and found through statistics that the control range of the fault with a drop of less than 5 m is about 30 m away from the pinch-out end of the fault. Guo et al. [25] analyzed the structural coal in nearly 60 coal and gas outburst cases in the Jiulishan mine of a coking coal group and found that structural coal accounted for 82.7%, indicating that the existence of structural coal has great risk of causing coal and gas outbursts. Shu et al. [26, 27] studied the 3rd coal seam of the Shitai coal mine in the Huaibei mining area and found that fault structure plays an obvious role in controlling gas content.

Cui and Yao [28] found that the fault has a controlling effect on the nonuniformity of gas occurrence and nonequilibrium of gas drainage in the coal seam on the working face, and there is a large gas pressure gradient between the two coal seams on the fault, leading to coal and gas outbursts. Zuo et al. [29, 30] according to the phenomena of coal and gas outburst induced by fault activation under dynamic disturbance. Based on the theory of fold mutation, the mechanical model of fault and surrounding rock mechanics was established, and the influencing factors of coal and gas outbursts were analyzed by introducing a dynamic disturbance factor. Zhao and Lei [31] think that in coal and gas explosions, the penetration of the plastic zone caused by high pressure gas storage and excavation disturbance is a necessary condition, and the mutation of the velocity field, displacement field, and stress field in the plastic zone is a sufficient condition. Zhao et al. [32] concluded that tectonic soft coal is mainly formed on the fault top wall under the effect of the fault structure. He and Chen [33] and Wei and Yao [34] discovered that the compressoshear fault formed because of large compressive stresses has a good effect on sealing the gas and is most beneficial to the occurrence of coal and gas outbursts. On the contrary, the extensional fault is conducive to releasing coal seam gas and not conducive to the occurrence of protrusion. The research of Jia et al. [35] found that as the angle between the fault strike and the direction of the stope main stress increases, the prominent hazard range also increases. With the heading of the working face toward the fault, the tectonic stress and the stope stress near the fault both form a relatively high concentrated stress, which is conducive to the formation of large protrusions [36, 37]. Wang [38] found that coal and gas outbursts are more likely to happen when the working face moves from the top wall to the footwall.

However, considering the difficulty in accurately identifying small faults [39, 40] (faults with a drop less than 5 meters) and the low gas content of coal seams in the mining area after gas drainage, it is difficult to let the coal and gas outburst accidents happen in the mining face [41]. Currently, for small faults, there are few studies on the control action of the minor faults' drop and trend on the coal and gas outburst in the mining face.

In the study of scholars like Huang et al. [42] and Wang and Lv [43], a fault with a drop of less than 5 meters was selected for study. However, the existing technology is not mature enough and the interference of different geological conditions makes it difficult to identify small faults with a fault spacing of about 3-5 m. Therefore, this paper selects the fault with a drop of less than 5 m (or even slightly more than 5 m) as a small fault to study the influence of small faults on coal and gas outbursts in the process of working face mining.

In this paper, the coal and gas outburst of the 2143_1 mining face of a mine are taken as the research object. The 3DEC three-dimensional discrete element numerical simulation method is used to analyze the control effect of different drops and different trends on the coal and gas outburst in the mining face during the coal seam mining process, in order to improve the effectiveness and pertinence of the mining face antiburst measures under the influence of small faults.

2. Mechanical Analysis of Fault Plane

The force model of a fault plane is established in a three-dimensional Cartesian coordinate system, as shown in Figure 1. The plane *ABCD* is the simplification of the fault plane, and the *X*, *Y*, and *Z* axes are, respectively, parallel to the maximum horizontal principal stress σ_2, the minimum horizontal principal stress σ_3, and the vertical principal stress σ_1. The line segment *OE* is the line connecting the intersection point *E* of the outer normal line of the plane *ABCD* with the fault plane and the origin *O*, and the angles with the *X*, *Y*, and *Z* coordinate axes are α, β, and γ, respectively.

For the stress analysis of the fault plane, the normal stress σ_n and the shear stress τ on the fault plane are the resultant force of the vertical principal stress σ_1, the maximum horizontal principal stress σ_2, and the minimum horizontal principal stress σ_3 in the normal direction of the fault plane and the resultant force of the components on the fault plane.

According to the principle of force synthesis, the resultant normal stress σ_n of the vertical principal stress σ_1 and the maximum horizontal principal stress σ_2 and the minimum horizontal principal stress σ_3 on the fault plane are

$$\sigma_n = \sigma_1' + \sigma_2' + \sigma_3' = \sigma_1 \times \cos^2\gamma + \sigma_2 \times \cos^2\alpha + \sigma_3 \times \cos^2\beta. \quad (1)$$

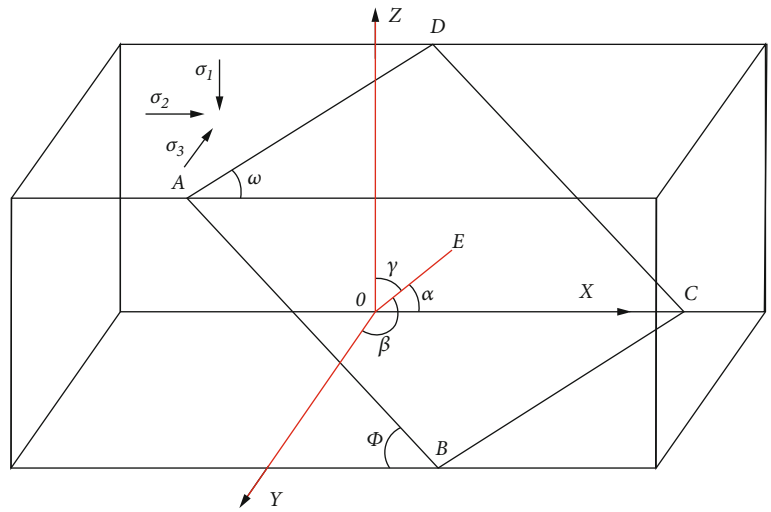

Figure 1: Mechanical model of fault plane.

Because of the different directions of shear stress components, the results of force synthesis are as follows:

$$\tau^2 = \sigma_1^2 \cos^2\gamma + \sigma_2^2 \cos^2\alpha + \sigma_3^2 \cos^2\beta - \sigma_n^2. \tag{2}$$

Among them, the vertical principal stress σ_1 mainly depends on the burial depth. Then,

$$\sigma_1 = \int_0^H \gamma(h)dh = \bar{\rho}gH, \tag{3}$$

where $\bar{\rho}$ is the average density of the overlying strata, kg/m^3; H is the burial depth, m; and g is the gravitational acceleration, 9.8 m/s^2.

Because of the existence of pores in the rock mass, gas exists in the pores of the rock mass, which produces pressure on the pores. Considering the existence of gas, pore pressure (P) is introduced here, and the horizontal principal stress includes the axial horizontal tectonic stress (σ_x and σ_y), the horizontal stress component(σ_h) of vertical stress (σ_1), and formation pore pressures (P); the maximum horizontal principal stress and the minimum horizontal principal stress σ_2 and σ_3, respectively, can be expressed as

$$\begin{cases} \sigma_2 = \sigma_h + \sigma_x + \dfrac{1-2\mu}{1-\mu}\delta p, \\ \sigma_3 = \sigma_h + \sigma_y + \dfrac{1-2\mu}{1-\mu}\delta p, \end{cases} \tag{4}$$

where σ_h is the horizontal component of the vertical stress σ_1, MPa; σ_x is the component of the tectonic stress along the X axis direction, MPa; σ_y is the component of the tectonic stress along the Y axis direction, MPa; μ is Poisson's ratio of the rock material; δ is the Biot coefficient; and the horizontal stress component (σ_h) of the vertical stress (σ_1) is

$$\sigma_h = \sigma_1\left(\frac{\mu}{1-\mu}\right)^{1/n}, \tag{5}$$

where n is the ratio of p to σ_n, which is a constant.

Substituting equations (3)–(5) into equations (1) and (2), the normal stress and shear stress formulas on the fault plane can be obtained:

$$\begin{cases} \sigma_n = (\sigma_x + B)\cos^2\alpha + (\sigma_y + B)\cos^2\beta + \bar{\rho}gH\cos^2\gamma, \\ \tau^2 = (\sigma_x + B)^2\cos^2\alpha + (\sigma_y + B)^2\cos^2\beta + (\bar{\rho}gH)^2\cos^2\gamma - \sigma_n^2, \end{cases} \tag{6}$$

where

$$B = \bar{\rho}gH\left(\frac{\mu}{1-\mu}\right)^{1/n} + \frac{1-2\mu}{1-\mu}\delta p. \tag{7}$$

If there is no fluid flow system (no gas flow), then the maximum horizontal principal stress and the minimum horizontal principal stress σ_2 and σ_3, respectively, can be expressed as

$$\begin{cases} \sigma_2 = \sigma_h + \sigma_x, \\ \sigma_3 = \sigma_h + \sigma_y. \end{cases} \tag{8}$$

Formula (7) is changed to

$$B = \rho gH\left(\frac{\mu}{1-\mu}\right)^{1/n}. \tag{9}$$

In addition, the relationship between the dip angle φ of the fault plane, the cross-section of the section, and the sharp angle ω of the maximum horizontal principal stress can also be obtained from Figure 1:

$$\begin{cases} \cos^2\alpha = \sin^2\phi \cdot \sin^2\omega, \\ \cos^2\beta = \sin^2\phi \cdot \cos^2\omega. \end{cases} \tag{10}$$

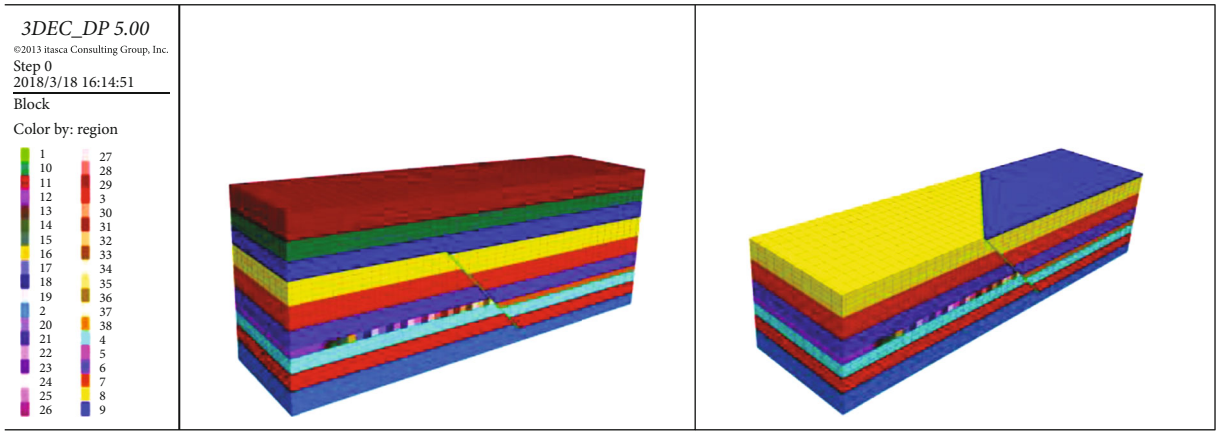

Figure 2: Numerical calculation model diagram of coal and gas outburst on mining face.

Bring it into equation (6) to get

$$\begin{cases} \sigma_n = \bar{\rho}gH + \left(\sigma_x - \sigma_y\right)\sin^2\phi \cdot \sin^2\omega + \left(\sigma_y + B - \bar{\rho}gH\right)\sin^2\phi, \\ \tau^2 = \left[\left(\sigma_x + B\right)^2 - \left(\sigma_y + B\right)^2\right]\sin^2\phi \cdot \sin^2\omega + \left[\left(\sigma_y + B\right)^2 - \left(\bar{\rho}gH\right)^2\right]\sin^2\phi + \left(\bar{\rho}gH\right)^2 - \sigma_n^2. \end{cases} \tag{11}$$

The derivative of equation (11) with respect to the fault strike ω:

$$\begin{cases} \dfrac{\partial\sigma_n}{\partial\omega} = \left(\sigma_x - \sigma_y\right)\sin^2\phi\,\sin 2\omega, \\ \dfrac{\partial\left(\tau^2 - \sigma_n^2\right)}{\partial\omega} = \left[\left(\sigma_x + B\right)^2 - \left(\sigma_y + B\right)^2\right]\sin 2\omega. \end{cases} \tag{12}$$

Since σ_n is consistent with the trend of the three principal stresses, and $\sigma_x > \sigma_y$, so $\partial\sigma_n/\partial\omega > 0$, that is, the resultant normal stress σ_n on the fault plane is positively correlated with the fault strike ω; when $\omega = 90^\circ$, the normal stress σ_n is the largest. That is to say, when the angle between the fault strike and the maximum horizontal principal stress of the stope is larger, the fault stress is larger. At the same time, $\partial(\tau^2 - \sigma_n^2)/\partial\omega > 0$ can be obtained, which means that as the fault strike increases, the difference between the shear stress and the normal stress increases continuously, and the shear stress on the fault plane provides the power for the unstable sliding of the fault. The normal stress on the fault plane prevents the unstable sliding of the fault, so the risk of an unsteady fault slide is positively correlated with the fault strike. This is consistent with the relationship between outburst frequency and fault strike found by Jia et al. [35] through the collation of outburst accidents in the Hegang mining area. That is, with the increase of the angle between the fault strike and the maximum horizontal principal stress, the number of outbursts begins to increase.

3. Calculation Model and Scheme

3.1. Project Summary. The coal seam no. 1 of a mine in Henan province is located in the lower part of the lower Shanxi formation of the Permian system, and its roof features are as follows: the pseudoroof is mudstone with an average thickness of 0.3 m. The direct roof is sandy mudstone with an average thickness of 8.6 m. The old roof is largely occupied sandstone with a minimum thickness of 6.6 m, a maximum thickness of 12.7 m, and an average thickness of 11.6 m. The floor of coal seam II_1 is characterized by the following: the direct floor is gray-black sandy mudstone containing plant debris fossils, and the local facies changes into medium-fine-grained sandstone. The minimum thickness is 6.67 m, the maximum thickness is 15.69 m, and the average thickness is 7.8 m. The minimum thickness of the base is 5.5 m, the maximum thickness is 14.7 m, and the average thickness is 9.1 m. The 2143_1 working face of the coal seam is 102 m away from the lower gateway. In the process of advancing, the working face encounters a normal fault. The normal fault strike has an included angle of 42° with the lower gateway, the fault inclination angle is 53°, and the drop is about 4 meters.

3.2. Numerical Calculation Model. Based on mechanical analysis of the fault plane, the influence of small faults with different drop heights and different strike mining faces on coal and gas outbursts was studied, taking the 2143_1 mining face as the geological prototype; the small fault with drop heights of 1 m, 4 m, and 7 m; a strike of 90°; and an inclination angle of 53°; as well as with strikes of 42°, 65°, and 90°; an inclination angle of 53°; and a drop height of 4 m; all are selected and used for numerical simulation studies. A three-dimensional calculation model is established as shown in Figure 2 by using 3DEC numerical simulation software; the size of the model is 300 m × 80 m × 100 m.

The model has six free faces, in which the four sides and the bottom boundary of the model are fixed at zero speed by

Table 1: Numerical analysis of physical and mechanical parameters of coal rock stratum.

Lithology	Density (kg/m^3)	Bulk modulus (GPa)	Shear modulus (GPa)	Friction angle (°)	Cohesion (MPa)	Tensile strength (MPa)
Mudstone	2200	18.33	8.46	35	1.48	1.83
Sandy mudstone	2100	26.67	8.89	38	1.57	2.36
Medium sandstone	2300	21.67	10.00	34	2.97	2.4
Mudstone	2200	18.33	8.46	35	1.48	1.83
Fine sandstone	2300	21.21	10.94	34	2.4	2.6
Sandy mudstone	2100	26.67	8.89	36	1.57	2.36
Coal	1400	12.50	5.77	28	1.34	1.6
Sandy mudstone	2100	26.67	8.89	38	1.8	2.36
Medium sandstone	2300	21.67	10.00	34	2.97	2.4
Siltstone	2400	18.67	11.20	32	3.8	4

Table 2: Numerical analysis of joint parameters.

Stratum	Normal stiffness (GPa)	Shear stiffness (GPa)	Friction angle (°)	Cohesion (MPa)	Tensile strength (MPa)
Mudstone	1.5	0.8	15	0.2	2.3
Sandy mudstone	2	1	17	0.42	2.2
Medium sandstone	6	4	18	0.87	7.6
Mudstone	1.5	0.8	15	0.2	2.3
Fine sandstone	4	4	20	0.93	8.31
Sandy mudstone	1.5	1	12	0.14	1.02
Coal	0.3	0.1	12	0.14	1.02
Sandy mudstone	2	1	22	0.35	2.3
Medium sandstone	6	4	15	0.47	2.5
Siltstone	4	4	17	0.39	3.8

fetching a thin layer, and the top of the model is a stress boundary. The overburden load in the study area is simulated by loading the vertical stress at the top of the model, meanwhile loading the ground stress along the X axis and Y axis directions to simulate the horizontal principal stress. The numerical study area is a single coal seam mining with a buried depth of 450 m. An equivalent load of 9.68 MPa was loaded on the top boundary of the model.

The physical and mechanical parameters of the coal and rock required by digital simulation methods are generally measured from physical experiments. However, most of the original rock masses contain rich joints and weak surfaces, so that the physical and mechanical parameters of the original rock mass are generally smaller than those measured by physical experiments. Therefore, the mechanical parameters of the numerical simulation require weakening of physical experimental data, taking 1/2-1/20 of the measured data in the laboratory. The physical and mechanical parameters of the coal seams required for numerical simulation are shown in Tables 1 and 2.

3.3. Computed Scheme. The working face of the model has a length of 80 m, is arranged parallel to the Y axis direction, and is mined in the positive direction of the X axis. The mining height of the mining face is 4 m. The length of each mining in the calculation process is 5 m with the calculation of 3000 time-stepping per step. In order to reduce the influence of boundary stress, a 20 m protective coal column is left at the opening of the working face.

In order to study the risk of instable slide of small faults with different drops during the advancing process of the mining face, the shear stress and normal stress on the fault surface are monitored. At the same time, by monitoring the movement rate of rock near small faults, the energy transferred from surrounding rock to the coal seam under the influence of small faults is reflected. When studying the influence of small faults with different strikes on coal and gas outbursts, the stress and displacement changes in the same mining face are monitored.

Faults are usually described by propensity, inclination, and drop. The small fault in the coal and gas outburst case selected in this paper can be described as $132° < 53° H = 4$ m normal faults by the above three factors. Since the angle between the fault strike and the crossheading is 42°, in this numerical simulation, the direction of the crossheading is parallel with the direction of the maximum horizontal principal stress; therefore, the trend, inclination, and drop are used to describe the small fault studied in this paper. Then,

Table 3: Numerical simulation scheme.

Attitude of fault	Original (°)	Control group (°)	
Trend	42	65	90
Drop	4	1	7

the small fault in the coal and gas outburst case selected in this paper can also be described as a normal fault of 42° < 53° $H = 4$ m.

To discuss the influence of different small faults on coal and gas outbursts in the mining face, this chapter chose small faults with different strikes and drops as objects and studied the influence of different small faults on coal and gas outbursts. The scheme of numerical simulation in this paper is shown in Table 3.

4. Control Effect of Small Fault Drop on Coal Mining and Gas Outburst

4.1. Risk of Unsteady Small Fault Slip during Mining. Figures 3 and 4 show the variational rule of normal stress and shear stress on the small fault zones with different falling gaps during the process of working face mining. It can be seen from Figure 3 that the normal stress changes of small faults with different drops have obvious similarities, and both tend to increase first and then decrease. When the working face is within the range of 130-40 m from the small fault, the normal stress change on the small fault zone tends to be stable; when the working face is advanced to 40 m, the normal stress on the small fault begins to increase slowly; when the working face is 15 m away from the small fault, the normal stress increases sharply for the first time, indicating that the tectonic stress near the small fault affected by coal mining is initially released. When the working face is 10 m away from the small fault, the normal stress on the small fault zone increases sharply for the second time. The normal stress peaks of the small fault with the difference of 1 m, 4 m, and 7 m are 14.4 MPa, 15.6 MPa, and 18.05 MPa, respectively. After that, the normal stress on the small fault zone decreases rapidly.

It can be seen from Figure 4 that the variation law of the shear stress on the small fault zone is basically consistent with the evolution law of the normal stress of the small fault zone corresponding to the drop. The difference is that the shear stress on the small fault zone begins to increase in the range of 30 m-10 m from the small fault, and the rate of increase becomes faster with the advancement of the working face and reaches a peak at 10 m from the small fault. The shear stress peaks with drops of 1 m, 4 m, and 7 m were 9.2 MPa, 10.7 MPa, and 14.05 MPa, respectively.

Summarizing the variation of normal stress and shear stress on small fault zones with different drops, it can be found that when the working face was advanced to within 40 m-10 m from the fault, the tectonic stress of the small fault zone is gradually released, but the small fault has not been destabilized. The tendency to slide down the fault surface leads to an increase in the normal stress on the small fault zone. However, when the working surface is pushed within

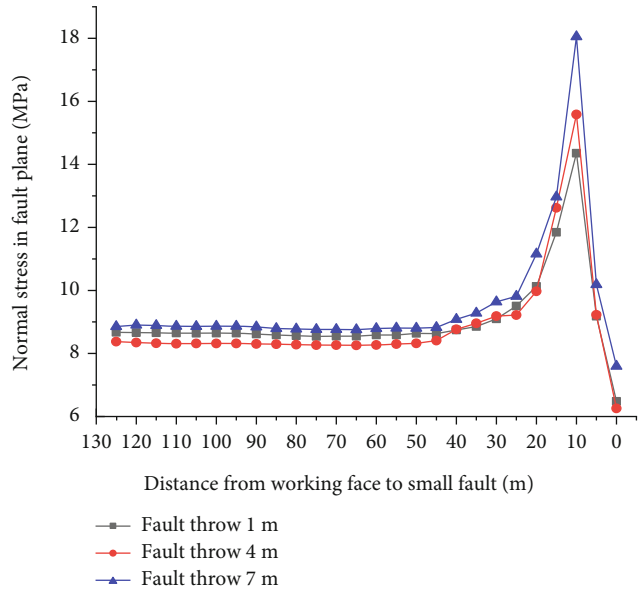

Figure 3: Influence of small fault drop on normal stress of fault plane. The black dotted line represents a fault throw of 1 m, the red dotted line represents a fault throw of 4 m, and the blue dotted line represents a fault throw of 7 m.

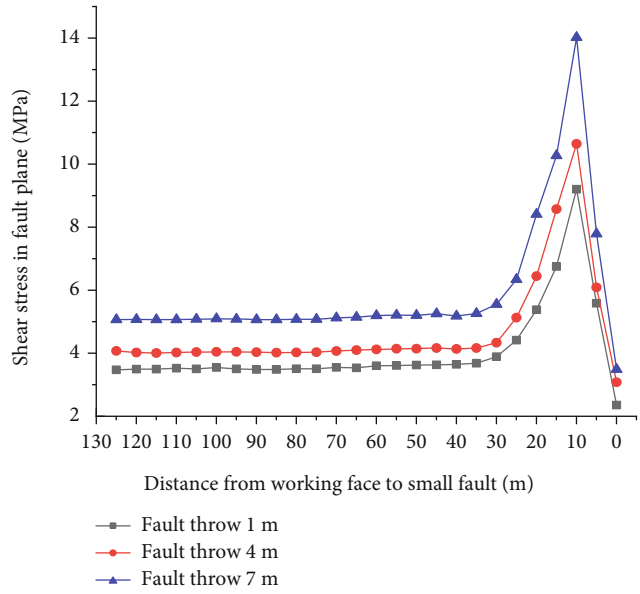

Figure 4: Influence of small fault drop on shear stress of fault plane. The black dotted line represents a fault throw of 1 m, the red dotted line represents a fault throw of 4 m, and the blue dotted line represents a fault throw of 7 m.

10 m of the small fault, the normal stress on the fault zone drops rapidly, indicating that the small fault begins to lose its stability and slip.

According to the Mohr-Coulomb failure criterion, the shear strength (τ_f) on the fault plane is

$$\tau_f = C_f + \sigma_n \tan \theta_f, \tag{13}$$

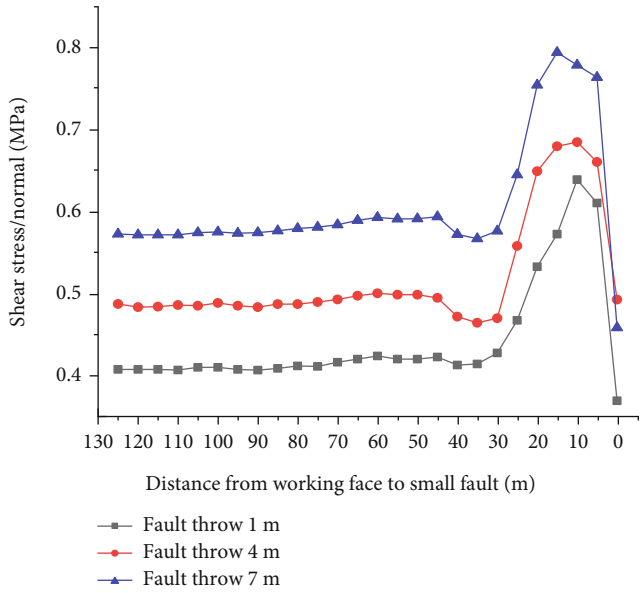

FIGURE 5: Influence of small fault drop on unsteady fault slide. The black dotted line represents a fault throw of 1 m, the red dotted line represents a fault throw of 4 m, and the blue dotted line represents a fault throw of 7 m.

where C_f and θ_f are the cohesion and internal friction angles of the fault plane rock mass, respectively.

According to equation (13), the slip motion of the small fault and the ratio of shear stress to compressive stress on the small fault zones are related. In order to consider the risk of small fault slip instability of different faults, the shear stress and normal stress data of small faults is processed to obtain the line diagram of the shear stress and normal stress ratio of small faults with different faults during the advancement of the working face, as shown in Figure 5.

It can be seen from Figure 5 that the ratio of the shear stress to the normal stress of each small fault is generally consistent with the trend of the work surface propulsion, and both tend to increase slowly-slowly decrease-rapidly increase-rapidly decrease. The ratio of shear stress to normal stress decreases slowly between 45 m and 30 m from the small fault. However, in the same range, the normal stress and shear stress of the small fault is increasing, indicating that the increase rate of the normal stress on the small fault zone is greater than the increase rate of the shear stress. When the working face is 30 m-10 m away from the small fault, the ratio of shear stress to normal stress increases rapidly and reaches a maximum when it is about 10 m away from the small fault, indicating that the coal mining face enters the influence range of the small fault zone, the increasing trend of shear stress on the fault zone dominates, and the risk of small fault instability and slip is greatest. For small faults with a drop of 1 m, 4 m, and 7 m, the peak values of the ratio of shear stress to normal stress are 0.64, 0.684, and 0.79, respectively. When the mining face is pushed to within 5 m from the fault, the ratio of shear stress to normal stress decreases rapidly, which is caused by the rapid decrease of shear stress and normal stress on the small fault plane. At this time, the small fault begins to lose stability and slip.

4.2. Influence of Small Fault Drop on Impact Energy of Overburden. Energy dissipation and energy release are important causes of rock mass failure [44–46]. When the small fault is unstable and sliding, the energy released by the small fault and the surrounding rock system consisting of the roof will be quickly transferred to the coal seam; assuming that the mass of the small fault zone and the roof plate system is m, the average velocity is v, and the time of energy release is t, the impact stress (F) and energy (W_{rock}) can be expressed as

$$\begin{cases} F = \dfrac{mv}{t}, \\ W_{\text{rock}} = \dfrac{1}{2} \cdot mv^2. \end{cases} \tag{14}$$

Since the impact time (t) is very small, the impact load (F) will be large. The energy released by the unstable coal rock mass contributes to the fracture of the coal body and creates favorable conditions for the occurrence of coal and gas outbursts.

According to equation (14), the energy released by the unit coal mass, i.e., the energy density w_{rock}, is as follows:

$$w_{\text{rock}} = \frac{1}{2} \cdot v^2. \tag{15}$$

According to equation (15), the amount of energy released by the unit coal rock mass can be judged by the velocity of the overlying strata near the small fault (v).

The upper parts of small faults are sliced, and the displacement change rate of overlying strata during the advancing process of the mining face is observed to judge the energy transferred to the coal seam when the small faults with different drops are unstable. According to the previous analysis, when the mining face is pushed to 5 m away from the small fault, and the small fault begins to slip, the displacement rate cloud map of overlying strata was analyzed, as shown in Figure 6.

It can be seen from Figure 6 that when the mining face is advanced to 5 m of a small fault, the overlying strata of the high velocity movement on the section are concentrated near the upper end of the fault. In addition, comparing the peaks of the displacement change rate of the overburden strata under the influence of small faults with drops of 1 m, 4 m, and 7 m, it can be found that the peak value of the displacement change rate increases with the increase of the drop. Under the influence of a small fault with a drop of 7 m, the peak value of the overburden movement rate is the largest, and the value reaches 0.689.

In order to more accurately compare the energy transferred from the surrounding rock to the coal seam under the influence of small faults with different drop differences, the roof of the coal seam 5 m away from the small fault is monitored, and a broken line chart of the rate change of

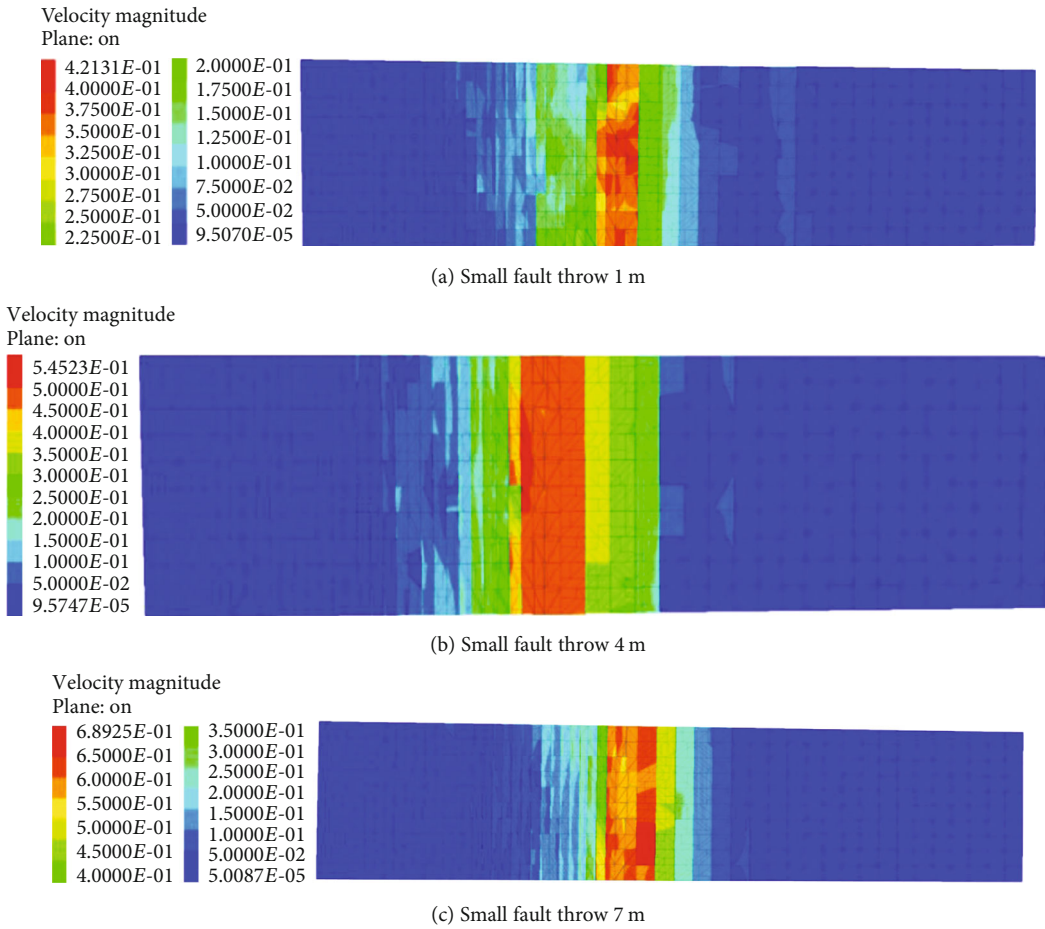

(a) Small fault throw 1 m

(b) Small fault throw 4 m

(c) Small fault throw 7 m

Figure 6: The displacement rate cloud map of the overburden layer when the mining face is advanced to the fault 5 m.

monitoring points during the advancing process of working face is drawn, as shown in Figure 7.

As can be seen from Figure 7, with the advancement of the working face, under the influence of small faults with different drops, the trend of the rate change of the monitored points is generally the same: when the working face is 130 m-35 m away from the fault, the rate of the monitored points changes little; when the fault is 35 m, the rate of the monitored point begins to increase significantly; and when the mining face advances below the monitoring point, the rate of the monitored point increases dramatically. Taking a small fault with a drop of 1 m as an example, when the mining surface is pushed below the monitored point, the rate of the monitored point increases from 0.56 to 1.48, an increase of 1.64 times.

Comparing the change of the velocity of the monitoring points under the influence of small faults with different drops, it can be seen that when the working face advances to within 20 m from the small fault and the drop of the small fault is 7 m, the rate change curve of the monitored points is always at the bottom of the three curves; at the top is the rate curve of the monitoring point under the influence of a small fault with a drop of 1 m.

Therefore, during the advancement of the mining face, when the small fault with a drop of 7 m is in the unstable slip, the surrounding rock transfers the most energy to the coal seam, which is most beneficial to the occurrence of coal and gas outbursts. When the drop is 1 m, the surrounding rock transfers the least energy to the coal seam, and the promotion of coal and gas outburst accidents is the weakest.

5. Controlling Effect of Strike of Small Fault on Coal and Gas Outburst in Mining Face

Figure 8 shows the velocity cloud diagram of the coal and rock mass when the working face is 5 m away from the fault under small fault control under different strikes. It can be seen from Figure 8 that due to the influence of the strike of small faults, the movement rate of the coal and seams along the inclination of the same mining face is not synchronized; as the strike of the small fault increases, the asynchronism of the change rate of coal and seam displacement gradually disappears in the dip direction of the working face, and when the strike of the small fault is perpendicular to the downward crossheading, the change rate of coal and seam displacement tends to be the same. At the same time, when the working surface is advanced to 5 m of the small fault, the range of violent activity of coal and rock increases with the increase of the trend of the small fault; the peak value of the movement rate of coal and rock decreases with the increase of the trend of

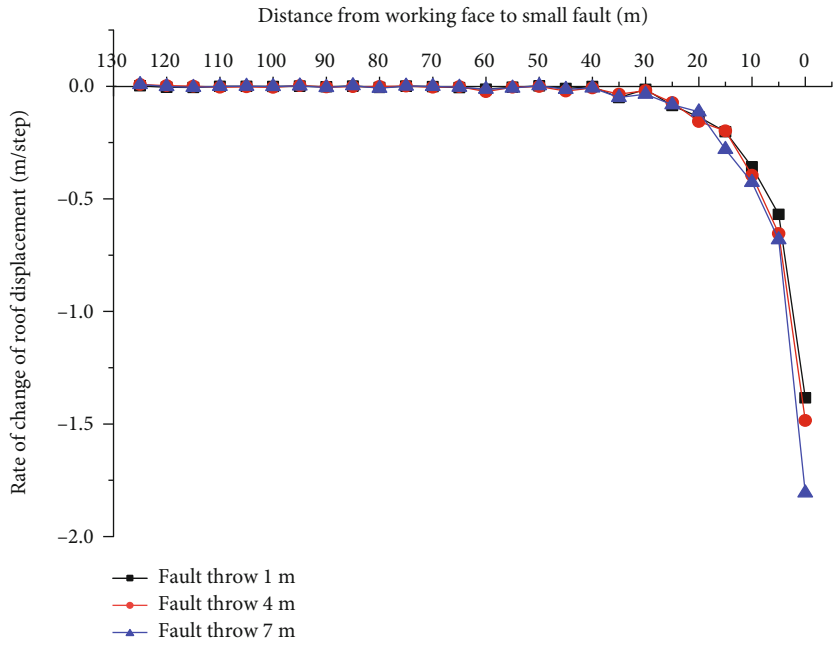

Figure 7: Rate curve of monitored points. The black dotted line represents a fault throw of 1 m, the red dotted line represents a fault throw of 4 m, and the blue dotted line represents a fault.

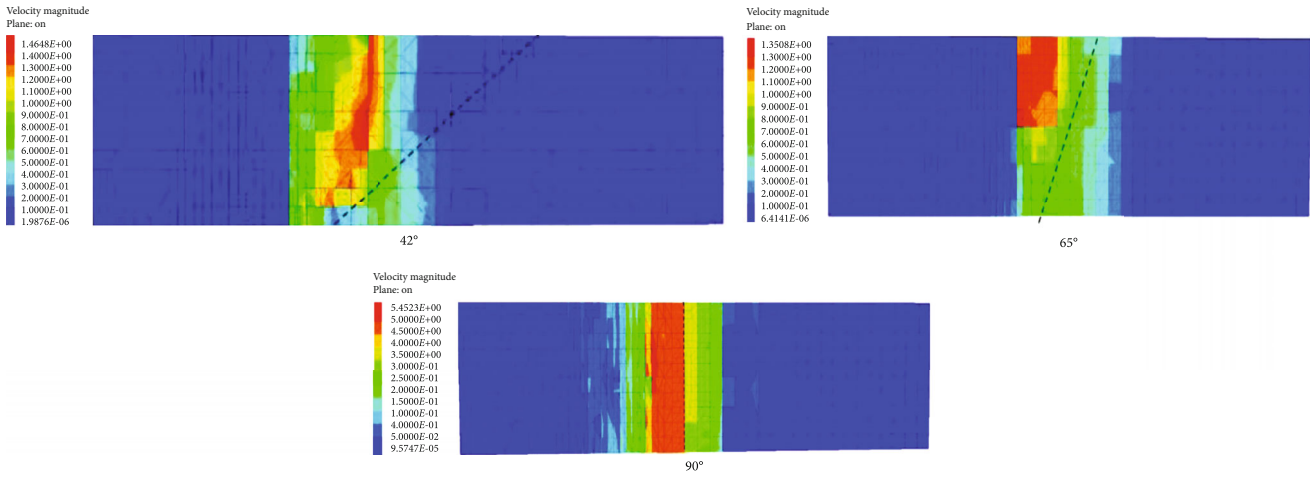

Figure 8: Rate cloud of coal and rock mass when the working face is 5 m away from the fault.

the small fault; when the small fault strikes at 42°, the peak velocity is 1.46, the peak velocity is 1.35 when the small fault strikes at 65°, and the peak velocity is 0.54 when the small fault strikes at 90°.

The coal and rock mass in the mining face is decompressed by deformation, so that the supporting stress of the mining face is transferred to the deep coal and rock mass. From the velocity cloud diagram under the influence of small faults with strikes of 42° and 65°, it can be found that the closer to the small fault, the smaller the movement rate of the coal and rock mass; on the contrary, the farther away from the small fault, the higher the movement rate of the coal and rock mass. It can be seen that the small fault destroys the continuity of the roof and hinders the transfer of the supporting stress of the mining face to the deep coal and rock mass, which will result in the smaller the distance from the dip direction of the same mining face to the small fault within the influence of the small fault, the greater the stress concentration of the coal and rock mass and the greater the risk of coal and gas outbursts.

Under the influence of three kinds of small faults with different strikes, when the mining face advances to 0 m of the small fault, the coal and rock mass with a unit cell at the boundary of the XZ plane along the dip direction of the mining face is taken as the monitoring point A, and the stress changes are monitored and compared, as shown in Figure 9. It can be found that under the control of three small faults with different strikes, the original stress of the monitoring point A decreases with the increase of the small fault strike; in addition, the stress peak of the monitoring point A increases with the increase of the small fault strike; when the small fault strikes at 42°, the stress peak is 37.2 MPa;

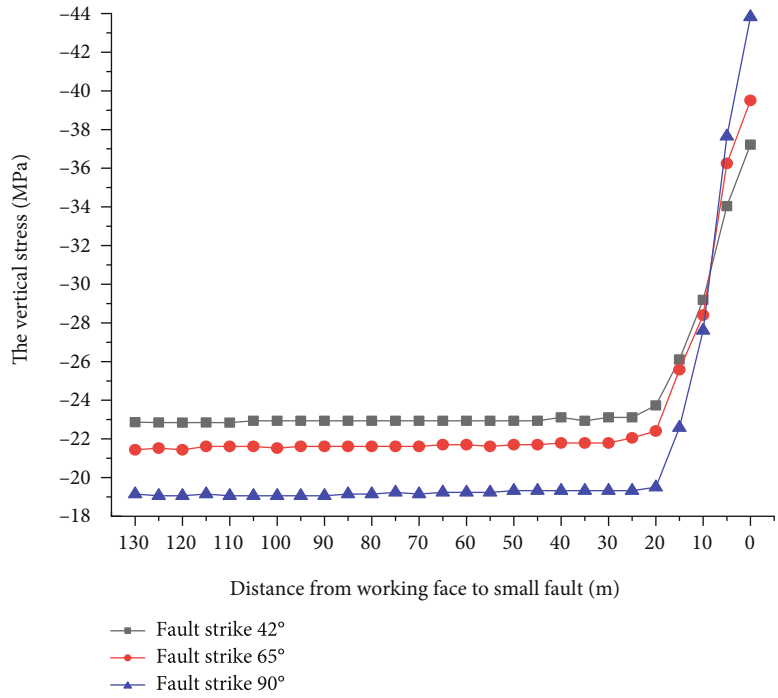

Figure 9: Line diagram of stress change at monitoring point A controlled by small fault with different strikes. The black dotted line represents a fault strike of 42°, the red dotted line represents a fault strike of 65°, and the blue dotted line represents a fault strike of 90°.

when the small fault strikes at 65°, the stress peak is 39.5 MPa; and when the small fault strikes at 90°, the stress peak is 43.8 MPa. Therefore, when the mining face is pushed into the range of influence of small faults, the larger the strike of the small fault, the greater the elastic potential of the coal rock mass stored in front of the face and the greater the possibility of protrusion.

6. Conclusion

(1) As the mining face is pushed into the influence of the small fault, the normal stress and shear stress on the small fault plane continue to increase with the advancement of the working face before the small fault undergoes unstable sliding. Among them, the increasing trend of shear stress is dominant, and the risk of small fault slip instability increases

(2) When the small fault slips and loses stability, the peak of the overlying rock movement rate near the small fault is positively correlated with the small fault drop. The energy transferred from the surrounding rock to the coal seam increases with the increase of the small fault drop. The larger the drop, the more the small fault slips. The greater the risk of displacement and instability, the more the impact of small faults on coal and gas outbursts in the working face increases with the increase in the drop

(3) The small fault hinders the transfer of the supporting stress of the mining face to the deep coal and rock mass, so that the movement of the same mining face along the dip direction of the small fault is not synchronized. The closer to the small fault, the greater the stress concentration of the coal and rock mass and the greater the risk of coal and gas outbursts

Data Availability

The data used to support the findings of this study are available from the first author upon request.

Conflicts of Interest

The authors declare that they have no conflict of interest.

Acknowledgments

This study was supported by the National Natural Science Foundation of China (51964007 and 51774101), the High Level Innovative Talents Training Project in Guizhou Province (Project No. 2016-4011), and the Guizhou Mining Power Disaster Early Warning and Control Technology Innovation Team Fund (Project No. 2019-5619).

References

[1] G. W. Dong and Q. T. Hu, "Main controlling geological body theory and geological effect mechanisms of coal and gas dynamic disaster," *Journal of Xi'an University of Science and Technology*, vol. 37, no. 1, pp. 7–14, 2017.

[2] X. Y. Shang and H. Tkalcic, "Point-source inversion of small and moderate earthquakes from P-wave polarities and P/S amplitude ratios within a hierarchical Bayesian framework: implications for the geysers earthquakes," *Journal of Geophysical Research-Solid Earth*, vol. 125, no. 2, 2020.

[3] T. Jia, Z. Feng, G. Wei, and Y. Ju, "Shear deformation of fold structures in coal measure strata and coal-gas outbursts: constraint and mechanism," *Energy Exploration & Exploitation*, vol. 36, no. 2, pp. 185–203, 2017.

[4] Y. B. Pan, "Gas geological occurrence regularity and coal and gas outburst research progress," *Fresenius Environmental Bulletin*, vol. 29, no. 3, pp. 1763–1770, 2020.

[5] E. Y. Wang, "Several problems of little faults study in coal mining," *China Mining Magazine*, vol. 15, no. 8, pp. 60–62, 2006.

[6] B. Wang, S. Liu, F. Zhou, J. Zhang, and F. Zheng, "Diffraction characteristics of small fault ahead of tunnel face in coal roadway," *Earth Sciences Research Journal*, vol. 21, no. 2, pp. 95–99, 2017.

[7] L. Chen, E. Wang, J. Ou, and J. Fu, "Coal and gas outburst hazards and factors of the no. B-1 coalbed, Henan, China," *Geosciences Journal*, vol. 22, no. 1, pp. 171–182, 2018.

[8] H. Wang, E. Y. Wang, and Z. H. Li, *Study on dynamic prediction model of gas emission in tunneling working face*, Combustion Science and Technology, 2020.

[9] A. Fisne and O. Esen, "Coal and gas outburst hazard in Zonguldak coal basin of Turkey, and association with geological parameters," *Natural Hazards*, vol. 74, no. 3, pp. 1363–1390, 2014.

[10] J. J. Zhang, K. L. Xu, G. Reniers, and G. You, "Statistical analysis the characteristics of extraordinarily severe coal mine accidents (ESCMAs) in China from 1950 to 2018," *Process Safety and Environmental Protection*, vol. 13, pp. 332–340, 2020.

[11] Y. K. Ma, B. S. Nie, X. Q. He, X. C. Li, J. Q. Meng, and D. Z. Song, "Mechanism investigation on coal and gas outburst: an overview," *International Journal of Minerals, Metallurgy and Materials*, vol. 27, no. 7, pp. 872–887, 2020.

[12] F. Du, K. Wang, X. Zhang, C. Xin, L. Shu, and G. Wang, "Experimental study of coal–gas outburst: insights from coal–rock structure, gas pressure and adsorptivity," *Natural Resources Research*, vol. 29, no. 4, pp. 2481–2493, 2020.

[13] D. Y. Xu and D. Y. Guo, "Dome-basin structure and its influence on coal and gas outbursts," *Polish Journal of Environmental Studies*, vol. 27, no. 4, pp. 1823–1831, 2018.

[14] D. Y. Guo, D. X. Han, and X. Y. Wang, "Outburst-prone tectonophisical environment and its application," *Journal of University of Science and Technology Beijing*, vol. 24, no. 6, pp. 581–584, 2002.

[15] B. Zhou, J. Xu, S. Peng et al., "Influence of geo-stress on dynamic response characteristics of coal and gas outburst," *Rock Mechanics and Rock Engineering*, 2020.

[16] K. Peng, J. Zhou, Q. Zou, Y. Zhang, and G. Tan, "Deformation characteristics and failure modes of sandstones under discontinuous multi-level cyclic loads," *Powder Technology*, vol. 373, pp. 599–613, 2020.

[17] F. X. Nie, H. L. Wang, and L. M. Qiu, "Research on the disaster-inducing mechanism of coal-gas outburst," *Advances in Civil Engineering*, vol. 2020, Article ID 1052618, 12 pages, 2020.

[18] K. Peng, J. Q. Zhuo, Q. L. Zuo, and X. Song, "Expansionary evolution characteristics of plastic zone in rock and coal mass ahead of excavation face and the mechanism of coal and gas outburst," *International Journal of Fatigue*, vol. 131, 2020.

[19] H. T. Liu, L. F. Guo, and X. D. Zhao, "Expansionary evolution characteristics of plastic zone in rock and coal mass ahead of excavation face and the mechanism of coal and gas outburst," *Energies*, vol. 13, no. 4, 2020.

[20] R. L. Zhang and I. S. Lowndes, "The application of a coupled artificial neural network and fault tree analysis model to predict coal and gas outbursts," *International Journal of Coal Geology*, vol. 84, no. 2, pp. 141–152, 2010.

[21] C. Zhai, X. Xiang, J. Xu, and S. Wu, "The characteristics and main influencing factors affecting coal and gas outbursts in Chinese Pingdingshan mining region," *Natural Hazards*, vol. 82, no. 1, pp. 507–530, 2016.

[22] W. Gong and D. Guo, "Control of the tectonic stress field on coal and gas outburst," *Applied Ecology and Environmental Research*, vol. 16, no. 6, pp. 7413–7433, 2018.

[23] W. Wang, X. Wang, and J. Yan, "The main factor controlling the coal and gas outbursts in the eastern Pingdingshan mining area," *Geotechnical and Geological Engineering*, vol. 34, no. 6, pp. 1825–1834, 2016.

[24] M. Chen, Q. H. Zhang, and Q. X. Wang, "Effect on scope of coal and gas outburst by fault," *Coal Science and Technology*, vol. 42, no. 3, pp. 39–41, 2014.

[25] D. Y. Guo, M. J. Zheng, C. Guo, D. M. Hu, and X. K. Zhang, "Extension clustering method for coal and gas outburst prediction and its application," *Journal of China Coal Society*, vol. 34, no. 6, pp. 39–41, 2009.

[26] L. Y. Shu, Y. P. Cheng, L. Wang, J. Y. Jiang, Q. W. Zhai, and S. L. Kong, "Research on influence of geological factors on gas storage in coal seam," *China Safety Science Journal*, vol. 21, no. 2, pp. 121–125, 2011.

[27] S. Longyong, W. Kai, Q. Qingxin, F. Shaowu, Z. Lang, and F. Xisheng, "Key structural body theory of coal and gas outburst," *Chinese Journal of Rock Mechanics and Engineering*, vol. 36, no. 2, pp. 347–356, 2017.

[28] H. Q. Cui and N. G. Yao, "Impermeable faults and prevention of gas hazards," *Journal of China Coal Society*, vol. 35, no. 9, pp. 1486–1489, 2010.

[29] M. L. Yu, Y. J. Zuo, H. Wang et al., "Study on the catastrophe theory of coal and gas outburst induced by dynamic disturbance," *Mining Research and Development*, vol. 38, no. 8, pp. 88–92, 2018.

[30] Y. Zuo, H. Wang, M. Yu, X. Dou, Z. Wu, and J. Wang, "Study on catastrophe theory of activation-induced prominence of faults under dynamic disturbance," *Advances in Civil Engineering*, vol. 38, no. 8, pp. 88–92, 2018.

[31] Z. D. Zhao and Y. Lei, "Mechanism analysis of uncovering coal in crosscut and gas outburst based on *Flac3D*," *Journal of Coastal Research*, vol. 103, pp. 333–338, 2020.

[32] W. F. Zhao, J. L. Xiong, J. Zhang, and M. Y. Ran, "Structure coal distribution law and affected to coal and gas outburst in Sichuan coal mining area," *Coal Science and Technology*, vol. 41, no. 2, pp. 52–55, 2013.

[33] J. He and X. S. Chen, "Research state and its development trends for control function of geological structure to coal and gas outburst," *Journal of Henan Polytechnic University*, vol. 28, no. 1, pp. 1–7, 2009.

[34] G. Y. Wei and N. G. Yao, "Characteristic of gas-geology at coal seam fault and its association with coal-gas outburst," *Journal of Liaoning Technical University*, vol. 31, no. 5, pp. 604–608, 2012.

[35] T. R. Jia, W. Wang, Z. M. Zhang, Z. H. Tan, and Y. J. Zhang, "Influence of fault strike on gas outburst under modern tectonic stress field," *Journal of Mining & Safety Engineering*, vol. 30, no. 6, pp. 930–934, 2013.

[36] K. Gao, Z. G. Liu, and J. Liu, "Effect of geostress on coal and gas outburst in the uncovering tectonic soft coal by cross-cut," *Chinese Journal of Rock Mechanics and Engineering*, vol. 42, no. 2, pp. 305–312, 2015.

[37] C. Liu, S. Li, C. Cheng, and J. Xue, "Activation characteristics analysis on concealed fault in the excavating coal roadway based on microseismic monitoring technique," *International Journal of Mining Science and Technology*, vol. 27, no. 5, pp. 883–887, 2017.

[38] J. P. Wang, "Research on laws of coal and gas outburst of tectonic region in Pingdingshan mining area," *Zhongzhou Coal*, vol. 11, pp. 50–54, 2016.

[39] Z. Y. Sun, S. P. Peng, and G. G. Zou, "Automatic identification of small faults based on SVM and seismic data," *Journal of China Coal Society*, vol. 42, no. 11, pp. 2945–2952, 2017.

[40] J. Wang, J. Lu, and G. M. Yu, "A normal fault in coal seams with drop height less than 3 m can be identified in seismic exploration?," *Journal of China Coal Society*, vol. 35, no. 4, pp. 629–634, 2010.

[41] W. Q. Zhang, B. M. Shi, and C. M. Mu, "Experimental research on failure and energy dissipation law of coal under impact load," *Journal of Mining & Safety Engineering*, vol. 33, no. 2, pp. 375–380, 2016.

[42] B. X. Huang, C. Y. Liu, and J. L. Xu, "Effect of little fault in working face on water conducted fissure height," *Journal of China Coal Society*, vol. 34, no. 10, pp. 1316–1321, 2009.

[43] E. Y. Wang and C. Z. Lv, "Study on small and medium-sized faults in multi-seam mining," *Mining Safety & Environmental Protection*, vol. 4, pp. 26-27, 1999.

[44] K. Peng, S. Shi, Q. Zou, Y. Zhang, and G. Tan, "Gas permeability characteristics and energy evolution laws of gas-bearing coal under multi-level stress paths," *Natural Resources Research*, vol. 29, no. 5, pp. 3137–3158, 2020.

[45] K. Peng, Z. Liu, Q. Zou, Q. Wu, and J. Zhou, "Mechanical property of granite from different buried depths under uniaxial compression and dynamic impact: an energy-based investigation," *Powder Technology*, vol. 362, pp. 729–744, 2020.

[46] K. Peng, H. Lv, F. Z. Yan, Q. L. Zhou, X. Song, and Z. P. Liu, "Effects of temperature on mechanical properties of granite under different fracture modes," *Engineering Fracture Mechanics*, vol. 226, 2020.